Direct Correlation between Molecular Dynamics and Enzymatic Stability: A Comparative Neutron Scattering Study of Native Human Butyrylcholinesterase and its "Aged" Soman Conjugate

F. Gabel,[†*] P. Masson,[†] M.-T. Froment,[‡] B. P. Doctor,[§] A. Saxena,[§] I. Silman,[¶] G. Zaccai,[†‖] and M. Weik[†*]

[†]Laboratoire de Biophysique Moléculaire, Institut de Biologie Structurale Jean-Pierre Ebel, CEA-CNRS-UJF, Grenoble, France; [‡]Centre de Recherches du Service de Santé des Armées, Unité d'Enzymologie, La Tronche, France; [§]Division of Biochemistry, Walter Reed Army Institute of Research, Silver Spring, Maryland; [¶]Department of Neurobiology, Weizmann Institute of Science, Rehovot, Israel; and [‖]Institut Laue-Langevin, Grenoble, France

ABSTRACT An incoherent elastic neutron scattering study of the molecular dynamics of native human butyrylcholinesterase and its "aged" soman-inhibited conjugate revealed a significant change in molecular flexibility on an angstrom-nanosecond scale as a function of temperature. The results were related to the stability of each state as established previously by differential scanning calorimetry. A striking relationship was found between the denaturation behavior and the molecular flexibility of the native and inhibited enzymes as a function of temperature. This was reflected in a quantitative correlation between the atomic mean-square displacements on an angstrom-nanosecond scale determined by neutron spectroscopy and the calorimetric specific heat. By the application of a simple two-state model that describes the transition from a folded to a denatured state, the denaturation temperatures of the native and the inhibited enzyme were correctly extracted from the atomic mean-square displacements. Furthermore, the transition entropy and enthalpy extracted from the model fit of the neutron data were, within the experimental accuracy, compatible with the values determined by differential scanning calorimetry.

INTRODUCTION

The structure-function-dynamics-stability relationship has served as a valuable concept for describing the behavior of biological systems at the molecular level. In this study we employed neutron spectroscopy to directly probe the relationship between the molecular dynamics (MD) of human butyrylcholinesterase (HuBChE) and its stability. We compared the native enzyme with a covalent conjugate produced by reaction with the potent organophosphate nerve agent soman. Cholinesterases (ChEs) are well suited for performing such a comparison because their enhanced stability upon binding of inhibitors has been well characterized (1–3).

ChEs are members of the α/β-hydrolase-fold family (4). Butyrylcholinesterase (BChE, EC 3.1.1.8) is structurally and functionally very similar to acetylcholinesterase (AChE, EC 3.1.1.7) (5,6). The catalytic turnover number of ChEs is among the highest known, approaching the diffusion limit (7). Although its physiological role is still uncertain (8,9), the HuBChE in plasma is of pharmacological and toxicological importance because it hydrolyzes the ester bonds of drugs such as heroin, cocaine, and succinyldicholine, and can neutralize organophosphate and carbamate poisons by reacting with them to form covalent conjugates (10). Indeed, HuBChE can serve as a stoichiometric bioscavenger for protection against highly toxic organophosphorus nerve agents (11,12), and administration of high doses of HuBChE confers efficient protection against otherwise lethal doses of several nerve agents (13). ChEs provide a particularly suitable system for studying relationships among activity, ligand binding and/or covalent modification, unfolding, and thermal molecular fluctuations, for the following reasons:

1. It has been proposed that binding of an inhibitor modifies the MD of the ChEs. Tara et al. (14) compared atomic root mean-square fluctuations of free mouse AChE and its complex with huperzine A in a 1 ns MD simulation. Although the differences between the two simulations were small, their comparison suggested that binding of the inhibitor produces a decrease in global molecular flexibility.
2. Irreversible inhibition of ChEs by covalent modification of the active-site serine with the organophosphate, soman (pinacolyl methylphosphonofluoridate), produces a conjugate that subsequently loses its pinacolyl group, leading to a so-called ''aged'' conjugate in which a salt bridge between the organophosphonyl moiety covalently attached to Ser^{198} and His^{438} contributes to its stabilization, and prevents reactivation by the quaternary oximes that are routinely employed as antidotes for treatment of nerve agent intoxication (5,15). The salt bridge formed as a consequence of the ''aging'' reaction has been shown to markedly increase the conformational stability of HuBChE (16), raising the temperature of thermal denaturation from 63°C to 73°C (17).

To investigate whether the biochemical modifications produced upon modification by soman are reflected by changes in MD, we conducted a comparative neutron scattering study on native and soman-inhibited HuBChE over

Submitted September 3, 2008, and accepted for publication October 20, 2008.

*Correspondence: frank.gabel@ibs.fr or martin.weik@ibs.fr

Editor: Patrick Loria.

0006-3495/09/02/1489/6 $2.00

doi: 10.1016/j.bpj.2008.10.029

a broad temperature range (2). It was found that the MD on an angstrom-nanosecond scale of HuBChE in the native and inhibited states was identical below the denaturation temperature of the native enzyme ($T_{m,nat} = 63°C$). Above $T_{m,nat}$, the atomic mean-square displacements (MSDs) for native HuBChE were larger than those for the ''aged'' soman-HuBChE conjugate. These results were interpreted in terms of higher free energy of the unfolded state of the ''aged'' soman conjugate with respect to the unfolded state of native HuBChE (2). These results were obtained in a limited temperature range, which was above $T_{m,nat}$ but below the denaturation temperature of the ''aged'' conjugate ($T_{m,inhib} = 73°C$).

In this study we extended the previous incoherent elastic neutron scattering (IENS) measurements for native and soman-inhibited HuBChE beyond the denaturation temperature of the soman-inhibited (aged) HuBChE conjugate, with a special focus on the denaturation temperature window (48–84°C). By covering the denaturation temperature range of both species, we were able to correlate the atomic MSDs measured by neutron spectroscopy with the calorimetric heat flow as measured earlier by differential scanning calorimetry (DSC) (17). We found a striking correlation, as a function of temperature, between the microscopic atomic MSDs on an angstrom-nanosecond scale and the macroscopic heat flow.

MATERIALS AND METHODS

Enzyme purification and characterization

The tetrameric form of HuBChE was purified to homogeneity from outdated human plasma by use of an improved protocol based on that of Grunwald et al. (18) and employed in our earlier studies (2,19). The highly purified HuBChE was stored at 4°C after lyophilization from 10 mM sodium phosphate, pH 8.0. Sodium dodecyl sulfate/polyacrylamide gel electrophoresis in the presence of β-mercaptoethanol (20) revealed a dominant 85 kDa band, assigned to the HuBChE monomer, and a weaker band at ~170 kDa, assigned to a residual, nonreducible, covalent HuBChE dimer. Contamination by other plasma proteins was negligible. A batch of 280 mg of HuBChE was dialyzed against 25 mM ammonium acetate, pH 7.0. Since this buffer is completely volatile, lyophilization resulted in salt-free protein powder. We refer to the native batch in the following as nat-HuBChE. A sample of ~140 mg of this HuBChE preparation was inhibited with soman, as described by Masson and Goasdoue (16), before dialysis and lyophilization. Inhibition by soman involves a phosphonylation reaction followed by rapid loss of the pinacolyl group of the soman moiety. This secondary reaction produces the ''aged'' conjugate, which is resistant to reactivation by oximes (21). This ''aged'' conjugate is referred to as soman-HuBChE in the following. Both lyophilized powders (nat-HuBChE and soman-HuBuChE) were placed in aluminum sample containers ($30 \times 40 \times 0.2$ mm^3), dried for 2 days at atmospheric pressure over phosphorous pentoxide (P_2O_5), and weighed. The measured weights were taken as their dry weights ($h = 0$ g water/g dry powder, denoted by ''g/g'' in the following). The weights of the dry samples of nat-HuBChE and soman-HuBChE were 138.5 and 142.6 mg, respectively.

For the neutron scattering experiments, both dry samples were hydrated by water vapor exchange for 2 days over pure D_2O (= 100% relative humidity) at 25°C in a desiccator. The final water content was measured by weighing the samples shortly before the sample holders were closed, resulting in 0.30 and 0.29 g/g for nat-HuBChE and soman-HuBChE, respectively. To verify that no loss of material had occurred, the samples were weighed before and after the neutron scattering experiments. No weight loss was detected for either sample.

Neutron scattering experiments and raw data analysis

Neutron scattering experiments were carried out on the backscattering spectrometer IN16 at the Institut Laue-Langevin (ILL; Grenoble, France), at an energy resolution $\Delta E = 0.9$ μeV (full width at half-maximum), corresponding to a timescale of ~1 ns, and a wave vector transfer (Q-range) of 0.19–1.93 Å^{-1}. The elastic intensities were measured as a function of temperature in the range of 321–358 K (48–84°C) in ΔT steps of ~2 K, with a fixed energy window corresponding to the instrumental resolution at zero energy transfer. The temperature scan rate was 0.05°C/min. Isolated data points were recorded for each sample at 20 K for normalization purposes (see next section).

The transmission values measured were 0.94 and 0.92 for nat-HuBChE and soman-HuBChE, respectively. The scattered signals were corrected for container scattering, absorption, and instrumental resolution (determined by separate runs of the empty container and a vanadium sample) by a recent version of the ILL program ''SQW'' (22) that is based on the correction formula of Paalman-Pings coefficients (23). Since the transmission values were high, the raw data were not corrected for multiple scattering.

To ensure the absence of crystalline structures in the samples, we used the IN16 option to record a diffraction pattern in parallel to the energy-resolved elastic scattering (24). For both samples and at all measured temperature points, no Bragg peaks were observed that might correspond to crystalline structures of either water or salt.

Determination of atomic MSDs

For atomic motions that are confined to a volume inside the space-time resolution of the instrument, the scattered elastic intensities I_{el} can be described, at small Q-values, within the Gaussian approximation:

$$I_{el}(Q) = A \times \exp\left[-(1/6) \times \langle u^2 \rangle Q^2\right]. \quad (1)$$

Where $Q = (4\pi/\lambda) \times \sin(\Theta/2)$ represents the wave vector transfer for a given scattering angle, Θ, and neutron wavelength, λ, and A is a constant. In this definition, the MSD $\langle u^2 \rangle$ refer to the full amplitude of the atomic motions (25). To extract the MSD, the measured elastic intensities of each sample at a given temperature, T, and wave vector transfer, Q, $I_{el}(Q,T)$, were normalized to the respective elastic intensities at the lowest temperature (20 K) (Eq. 2). In our case, the MSD at 20 K is essentially zero, so that

$$I_{norm}(Q,T) = I_{el}(Q,T)/I_{el}(Q, T = 20\text{K}) = \exp\left[-(1/6) \times \langle u^2 \rangle_T Q^2\right]. \quad (2)$$

The normalized intensities were plotted on a semilogarithmic plot versus Q^2 (Fig. 1). We refer to these plots as ''Guinier plots'' because of their analogy to the Guinier plots in small angle scattering (26). MSDs were extracted from the slopes of linear regimes in the Q-range of 0.19 Å^{-2} < Q^2 < 1.13 Å^{-2}. The criterion for the validity of the Gaussian approximation, $\langle u^2 \rangle Q^2 \leq$ ~2, was reasonably fulfilled, with the maximum value for $\langle u^2 \rangle Q^2$ being 2.7.

The MSDs were plotted as a function of temperature (Fig. 2). In the ranges where the MSD varied linearly with temperature, linear fits were applied and effective force-constants were extracted according to the following equation (27):

$$\langle k' \rangle = 0.00276/\left(d\langle u^2 \rangle/dT\right). \quad (3)$$

In Eq. 3, $\langle k' \rangle$ is in N/m when $\langle u^2 \rangle$ is in Å^2, and T is in Kelvin. The respective temperature ranges for the linear fits were 48–63°C and 63–84°C for

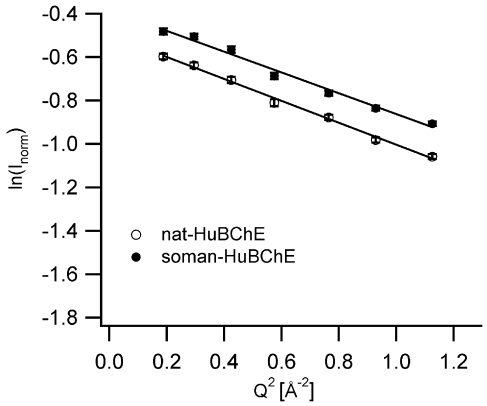

FIGURE 1 Logarithmic representation of the normalized intensities (Eq. 2) for nat-HuBChE and soman-HuBChE as a function of Q^2 at 84°C. The lines represent the linear fits used to extract the respective MSD.

nat-HuBChE, and 48–72°C and 72–84°C for soman-HuBChE (see also Fig. 2).

Denaturation described by an adapted double-well model

To relate the atomic MSDs measured by neutron spectroscopy to thermodynamic parameters, an adapted double-well potential was applied to fit the neutron data. In the model of Bicout and Zaccai (28), the dynamical transition of a protein is described by two harmonic potential wells separated by a free energy difference, ΔG_{trans}. Here, we assume that a second transition takes place at the denaturation onset temperature (which is far above the protein dynamical transition at ~200 K); we therefore extend the double-well model by adding a third potential well that represents the denatured state. It is separated by ΔG_{denat} from the native state and is populated only at very high temperatures. Furthermore, we assume, in the temperature range with which we are concerned (>320 K/47°C), that the first and second potential wells, below and above the protein dynamical transition, respectively, can be described by a single, combined potential well. We can then approximate the atomic MSD by the following equation:

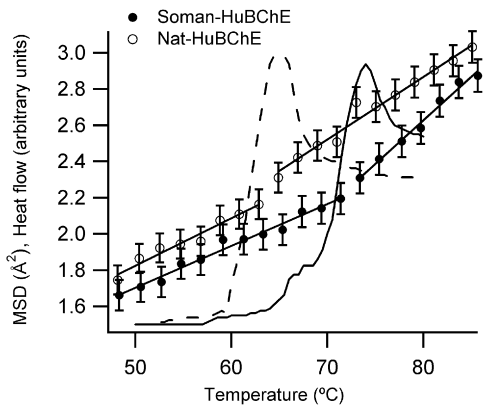

FIGURE 2 Overlay of MSDs and heat flows of nat-HuBChE (*broken line*) and soman-HuBChE (*continuous line*), measured by neutron spectroscopy and DSC (reproduced from Masson et al. (17)). The linear fits of the MSDs show inflection points at ~64°C and ~73°C for nat-HuBChE and soman-HuBChE, respectively. Effective force constants k_1 (Table 1) were extracted from these linear fits.

$$\langle u^2(T)\rangle = A + (1-\phi(T)) \times (k_B T)/k_1 + \phi(T) \times (k_B T)/k_2, \quad (4)$$

where $\phi(T)$ describes the population of atoms that are found, at a given temperature T, in the potential well with the higher free energy, i.e., in the denatured state. It can be expressed as a partition function (28):

$$\phi(T) = 1/(1 + \exp(\Delta G_{\text{denat}}/(k_B T))). \quad (5)$$

$\Delta G_{\text{denat}} = \Delta H - T\Delta S$ is the free energy difference between the native and denatured states. Its complement, $1 - \phi(T)$, describes the population of atoms that remain in the lower free energy potential well at a given temperature, i.e., in the nondenatured state. k_B is the Boltzmann constant, and k_1 and k_2 are effective force constants associated with the two energy potential wells (27). A is a phenomenological constant that takes into account that the linear fit of the MSD associated with the lower-energy potential well (effective force constant k_1) does not pass through zero for $T = 0$ K. Consequently, Eq. 4 neglects contributions from the lowest-energy potential well (the one below the protein dynamical transition) to the overall MSD at high temperatures.

MSDs from nat-HuBChE and soman-HuBChE were both fitted by Eq. 4 between 321 K (48°C) and 357 K (84°C), and the respective fit parameters ΔH, ΔS, k_2, and A were extracted for each data set. k_1 (the effective force constant for the nondenatured states) was not considered as a free fit parameter but as a fixed fit parameter. Its values were determined by linear fits using Eq. 3 in the temperature ranges of 48–63°C (nat-HuBChE) and 48–72°C (soman-HuBChE) (Fig. 2), and introduced as fixed parameters in Eq. 4 for both data sets. In the case of nat-HuBChE, we also used a variation of the fit described above to check its agreement with the DSC data (17) by imposing $\Delta H = 780$ kJ/mol as a fixed parameter. In all cases, the denaturation temperature, T_m, was determined as $T_m = \Delta H/\Delta S$.

RESULTS

Correlation between atomic MSDs and heat flow

Fig. 2 displays the MSDs of nat-HuBChE and soman-HuBChE as a function of temperature, measured by neutron spectroscopy in hydrated powders, superposed on DSC data obtained in solution in a previous study (17). The DSC data were recorded at a temperature scan rate of 0.1°C /min, comparable to that used in the neutron scattering experiments. It is of interest that the temperature dependence of the MSDs for nat-HuBChE and soman-HuBChE differed significantly from each other but correlated strongly with the corresponding DSC data. At temperatures below ~63°C, the MSDs of the two samples were comparable within experimental error, in agreement with our earlier results (2). Indeed, the linear fits (Eq. 3) below that temperature displayed similar effective force constants $k_1 = 0.107$ and 0.117 N/m for nat-HuBChE and soman-HuBChE, respectively, indicating that the atoms in both systems move in free energy potential wells of very similar geometry (29). These values were used as fixed parameters in Eq. 4 for the adapted double-well model (see below).

Above this temperature, however, the MSDs for nat-HuBChE increased more strongly than those for soman-HuBChE, as illustrated by the inflection in the linear fits displayed in Fig. 2. The latter started to increase only at

~73°C, in a fashion similar to those of its noninhibited counterpart at a temperature ~10°C lower. Most strikingly, the inflection points of the MSDs (i.e., the temperature at which they begin to increase at a higher rate) match quite well the respective melting temperatures, T_m, for nat-HuBChE (63°C) and soman-HuBChE (73°C), as determined by DSC in D_2O (17). Above the denaturation temperatures of both samples ($T > 80$°C), the two sets of MSDs tend to converge again, and increase at a similar rate. Above 80°C, the effective force constants of nat-HuBChE and soman-HuBChE are smaller (0.075 and 0.057 N/m, respectively) than they are below the denaturation temperature, and their free energy potential wells are shallower (27).

Fit of an adapted double-well model and comparison with thermodynamic data

Fig. 3 illustrates the fits of both experimental MSD data sets to the adapted double-well model (Eq. 4) with free enthalpy differences ΔH. The extracted parameters are shown in Table 1. Fig. 4 compares the fits of the nat-HuBChE MSDs with free ΔH and with $\Delta H = 780$ kJ/mol (the experimental value obtained from the DSC measurements) imposed as a fixed parameter.

As shown in Table 1, the fit of the atomic MSDs using an adapted double-well model reproduces semiquantitatively the thermodynamic parameters of HuBChE in solution as determined previously by DSC (17). Of great interest, the midpoint transition temperatures determined from the neutron scattering data obtained with the hydrated powder are in good agreement with the corresponding values determined by DSC in solution (67.5 vs. 63°C and 77.8 vs. 73°C for nat-HuBChE and soman-HuBChE, respectively). Although they are the right order of magnitude, the enthalpy differences extracted from the neutron data by means of Eq. 4 differ from those determined by DSC by a factor of about 2. However, our experimental neutron scattering data are still compatible with the thermodynamic parameters determined by DSC (Fig. 4, *broken line*). Although it yielded a slightly worse fit ($\chi^2 = 0.0265$ vs. 0.0199), an imposed enthalpy difference of 780 kJ/mol between the native and denatured states was in agreement with the qualitative behavior of the MSDs. Furthermore, it excellently reproduced the transition temperature T_m (65.8°C obtained from the neutron scattering data vs. 65°C obtained by DSC) that was kept as a free parameter during the fit procedure.

TABLE 1 Physical and thermodynamic parameters of HuBChE

	k_1 (*N*/m)	k_2 (*N*/m)	ΔS (J/mol·K)	ΔH (kJ/mol)	T_m (°C)	χ^2
nat-HuBChE (ΔH free)	0.107	0.104	1120	382	67.5	0.0199
nat-HuBChE (ΔH fixed)	0.107	0.104	2301	780	65.8	0.0265
soman-HuBChE (ΔH free)	0.117	0.112	1080	379	77.8	0.0103

Table 1 The parameters were extracted by fitting the MSD by the double-well model (Eq. 4) using a fixed parameter k_1 for both nat-HuBChE and soman-HuBChE.

DISCUSSION

MSDs are a measure of the atomic thermal fluctuations of biomacromolecules (25). Their amplitude can be related to the shape of the potential energy well within which the atoms of the macromolecule move (29). Moreover, their rate of increase with temperature can be related to a force constant (effective force constant at higher temperatures in a quasiharmonic approximation) of the potential well that confines the macromolecular atoms around an equilibrium position (27). Whereas a modest increase in MSD values with temperature represents a steep energy potential well, a more rapid increase of MSD with temperature is an indication of a shallow potential well. The absolute MSD values determine the width of the potential well. The temperature dependences of the atomic MSDs in this study are, therefore, a measure of how the structural changes produced by the covalent modification with soman, and the subsequent ''aging'' reaction, affect the mean potential energy landscape (29) of the atoms of HuBChE.

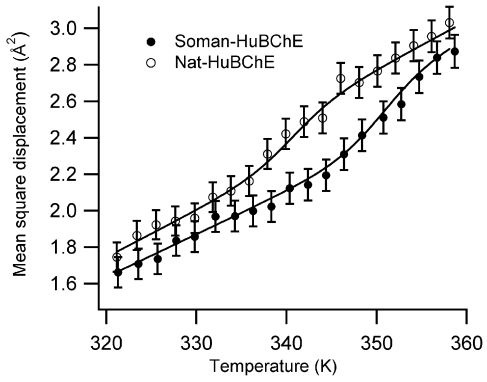

FIGURE 3 Fit of Eq. 4 to the experimental MSDs of nat-HuBChE and soman-HuBChE.

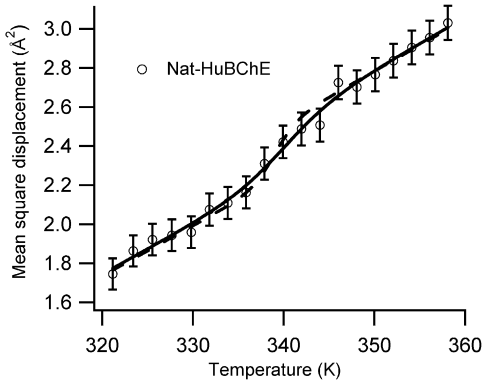

FIGURE 4 Fit of Eq. 4 with the experimental MSDs for nat-HuBChE. Comparison between fits with a free fit parameter ΔH (*continuous line*) and the experimental value obtained by DSC, $\Delta H = 780$ kJ/mol, imposed as a fixed parameter (*broken line*).

In these terms, the inhibitor does not affect the mean atomic potentials of HuBChE below 63°C, since both the absolute values of the MSDs as well as their rate of increase with temperature are indistinguishable, within experimental error, for nat-HuBChE and soman-HuBChE. These results are in agreement with our earlier data (2). At ~63°C, however, the MSDs of nat-HuBChE start to increase more rapidly with temperature than those of soman-HuBChE (Fig. 2). This serves as a general indication that the walls of the potential well are becoming shallower and the extension in space is increasing.

It is intriguing that the formation of a single salt bridge between the protonated active-site histidine and the covalently attached methylphosphonyl group within the active site produces both an increase in thermodynamic stability and a decrease in flexibility of the protein above 63°C. As previously suggested (17), partial desolvation of the active-site pocket may promote the formation of hydrophobic interactions within it and thereby induce rigidification of the whole protein structure.

In this study we compared neutron scattering data from hydrated enzyme powders with DSC data from enzymes in aqueous solution. The decision to work with a lyophilized powder rather than a solution was made for several reasons: First, the sample amount in the neutron beam is maximized, and consequently so is the signal/noise ratio. Second, global diffusion of macromolecules in powder is suppressed (30). Third, a minimal degree of hydration, together with very good energy resolution, minimizes quasielastic scattering contributions to the elastic signal, as required both for reasonable application of the Gaussian approximation (31) and for reasonable interpretation of our data in terms of a double-well model (28).

Although the adapted double-well model proposed here (Eq. 4) certainly represents an oversimplified view of protein dynamics, it is remarkable that the denaturation temperatures and, to a lesser degree, the enthalpies extracted from the neutron data agree well with the respective values determined by DSC. Since the shift in denaturation temperature between native and inhibited HuBChE is very pH-sensitive (17), it is likely that the pH conditions in the partially hydrated, lyophilized powders can be likened to those in solution. This effect is known as ''pH memory'', and was first described by Zaks and Klibanov (32). The excellent agreement between the denaturation temperatures in solution and in powders suggests that the denaturation process observed for both samples in solution, as measured by DSC, occurs similarly in the hydrated powders, and is reflected by an abrupt increase in the molecular atomic motions on an angstrom-nanosecond scale around the denaturation temperature.

CONCLUSIONS

We compared the atomic MSDs of nat-HuBChE and aged soman-HuBChE on an angstrom-nanosecond scale, as measured by neutron spectroscopy, with their respective denaturation behaviors, as measured by DSC. We found a direct correlation between the denaturation temperatures, T_m, of the two samples and an inflection point in the rate of increase in their respective molecular flexibilities, as indicated by the measured increases in their MSDs. We described the temperature behavior of the atomic MSDs by means of a simple double-well model and directly extracted from this microscopic information macroscopic thermodynamics parameters, such as denaturation temperatures, enthalpies, and entropies, that are in quantitative agreement with the DSC data.

We thank the IN16 staff (ILL, Grenoble, France), Dr. Bernhard Frick, Dr. Thilo Seydel, and Dr. Heloisa Bordallo for support during the neutron scattering experiments.

This study was supported by the European Union DLAB program under contract Nos. HPRI-CT-2001-50035 and RII3-CT-2003-505925. M.W. was supported by a grant from the Agence Nationale de la Recherche (project No. JC05_45685).

REFERENCES

1. Payne, C. S., M. Saeed, and A. D. Wolfe. 1989. Ligand stabilization of cholinesterases. *Biochim. Biophys. Acta.* 999:46–51.
2. Gabel, F., M. Weik, P. Masson, F. Renault, D. Fournier, et al. 2005. Effects of soman inhibition and of structural differences on cholinesterase molecular dynamics: a neutron scattering study. *Biophys. J.* 89:3303–3311.
3. Rochu, D., C. Clery-Barraud, F. Renault, A. Chevalier, C. Bon, et al. 2006. Capillary electrophoresis versus differential scanning calorimetry for the analysis of free enzyme versus enzyme-ligand complexes: in the search of the ligand-free status of cholinesterases. *Electrophoresis.* 2:442–451.
4. Ollis, D. L., E. Cheah, M. Cygler, B. Dijkstra, F. Frolow, et al. 1992. The α/β-hydrolase fold. *Protein Eng.* 5:197–211.
5. Nicolet, Y., O. Lockridge, P. Masson, J. C. Fontecilla-Camps, and F. Nachon. 2003. Crystal structure of human butyryl cholinesterase and of its complexes with substrate and products. *J. Biol. Chem.* 278:41141–41147.
6. Silman, I., and J. L. Sussmann. 2005. Acetylcholinesterase: 'classical' and 'non-classical' functions and pharmacology. *Curr. Opin. Pharmacol.* 5:293–302.
7. Quinn, D. M. 1987. Acetylcholinesterase: enzyme structure, reaction dynamics, and virtual transition states. *Chem. Rev.* 87:955–979.
8. Darvesh, S., D. A. Hopkins, and C. Geula. 2003. Neurobiology of butyrylcholinesterase. *Nat. Rev. Neurosci.* 4:131–138.
9. Duysen, E. G., B. Li, S. Darvesh, and O. Lockridge. 2007. Sensitivity of butyrylcholinesterase knockout mice to (−)-huperzine A and donepezil suggests humans with butyrylcholinesterase deficiency may not tolerate these Alzheimer's disease drugs and indicates butyrylcholinesterase function in neurotransmission. *Toxicology.* 233:60–69.
10. Li, B., M. Sedlacek, I. Manoharam, R. Boopathy, E. G. Duysen, et al. 2005. Butyrylcholinesterase, paraoxonase, and albumin esterase but not carboxylesterase, are present in human plasma. *Biochem. Pharmacol.* 70:1673–1684.
11. Doctor, B. P., and A. Saxena. 2005. Bioscavengers for the protection of humans against organophosphate toxicity. *Chem. Biol. Interact.* 157–158:167–171.
12. Huang, Y. -J., Y. Huang, H. Baldassarre, B. Wang, A. Lazaris, et al. 2007. Recombinant human butyrylcholinesterase from milk of transgenic animals to protect against organophosphate poisoning. *Proc. Natl. Acad. Sci. USA.* 104:13603–13608.
13. Ashani, Y., and S. Pistinner. 2004. Estimation of the upper limit of human butyrylcholinesterase dose required for protection against

organophosphates toxicity: a mathematically based toxicokinetic model. *Toxicol. Sci.* 77:358–367.

14. Tara, S., T. P. Straatsma, and J. A. McCammon. 1999. Mouse acetylcholinesterase unliganded and in complex with huperzine A: a comparison of molecular dynamics simulations. *Biopolymers.* 50:35–43.
15. Millard, C. B., G. Kryger, A. Ordentlich, H. M. Greenblatt, M. Harel, et al. 1999. Crystal structures of aged phosphorylated acetylcholinesterase: nerve agent reaction products at the atomic level. *Biochemistry.* 38:7032–7039.
16. Masson, P., and J. Goasdoue. 1986. Evidence that the conformational stability of ''aged'' organophosphate-inhibited cholinesterase is altered. *Biochim. Biophys. Acta.* 14:304–313.
17. Masson, P., C. Cléry, P. Guerra, A. Redslob, C. Albaret, et al. 1999. Hydration change during the aging of phosphorylated human butyrylcholinesterase: importance of residues aspartate-70 and glutamate-197 in the water network as probed by hydrostatic and osmotic pressures. *Biochem. J.* 343:361–369.
18. Grunwald, J., D. Marcus, Y. Papier, L. Raveh, Z. Pittel, et al. 1997. Large-scale purification and long-term stability of human butyrylcholinesterase: a potential bioscavenger drug. *J. Biochem. Biophys. Methods.* 34:123–135.
19. Gabel, F., M. Weik, B. P. Doctor, A. Saxena, D. Fournier, et al. 2004. The influence of solvent composition on global dynamics of human butyrylcholinesterase powders: a neutron scattering study. *Biophys. J.* 86:3152–3165.
20. Laemmli, U. K. 1970. Cleavage of structural proteins during the assembly of the head of bacteriophage T4. *Nature.* 227:680–685.
21. Millard, C. B., and C. A. Broomfield. 1995. Anticholinesterases: medical applications of neurochemical principles. *J. Neurochem.* 64:1909–1918.
22. Anderson, I. S., and R. Nelson. 1985. User's Guide for Program 'SQW'. Institut Laue-Langevin Internal Report No. ILL85AN8T, Grenoble, France.
23. Bée, M. 1988. Quasielastic Neutron Scattering. Adam Hilger, Bristol, UK.
24. Combet, J., B. Frick, O. Losserand, M. Gamon, and B. Guerard. 2000. Simultaneous diffraction and inelastic scattering on the backscattering instrument IN16. *Phys. B Cond. Matt.* 283:380–385.
25. Smith, J. C. 1991. Protein dynamics: comparison of simulations with inelastic neutron scattering experiments. *Q. Rev. Biophys.* 24: 227–291.
26. Guinier, A., and G. Fournet. 1955. Small Angle Scattering of X-Rays. John Wiley & Sons, New York, London.
27. Zaccai, G. 2000. How soft is a protein? A protein dynamics force constant measured by neutron scattering. *Science.* 288:1604–1607.
28. Bicout, D. J., and G. Zaccai. 2001. Protein flexibility from the dynamical transition: a force constant analysis. *Biophys. J.* 80:1115–1123.
29. Frauenfelder, H., F. Parak, and R. D. Young. 1988. Conformational substrates in proteins. *Annu. Rev. Biophys. Biophys. Chem.* 17:451–479.
30. Perez, J., J. -M. Zanotti, and D. Durand. 1999. Evolution of the internal dynamics of two globular proteins from dry powder to solution. *Biophys. J.* 77:454–469.
31. Gabel, F. 2005. Protein dynamics in solution and powder measured by incoherent elastic neutron scattering: the influence of Q-range and energy resolution. *Eur. Biophys. J.* 34:1–12.
32. Zaks, A., and A. M. Klibanov. 1985. Enzyme-catalyzed processes in organic solvents. *Proc. Natl. Acad. Sci. USA.* 82:3192–3196.